

## Article

# Development and First Results of a No-Till Pneumatic Seeder for Maize Precise Sowing in Huang-Huai-Hai Plain of China

Hui Li <sup>1</sup>, Hu Liu <sup>1</sup>, Jilei Zhou <sup>1</sup>, Guojian Wei <sup>1</sup>, Song Shi <sup>1,\*</sup>, Xiangcai Zhang <sup>2</sup>, Rongfang Zhang <sup>1</sup>, Huibin Zhu <sup>3</sup> and Tengfei He <sup>1</sup>

<sup>1</sup> Shandong Academy of Agricultural Machinery Sciences, Jinan 250010, China; lihuictc@163.com (H.L.); liuhu0725@163.com (H.L.); zhoujilei@shandong.cn (J.Z.); woshitxwh@126.com (G.W.); zhangrongfang06@126.com (R.Z.); hetengfei.1@163.com (T.H.)

<sup>2</sup> School of Agricultural Engineering and Food Science, Shandong University of Technology, Zibo 255000, China; zxcai0216@163.com

<sup>3</sup> Faculty of Modern Agricultural Engineering, Kunming University of Science and Technology, Kunming 650500, China; hbzhu113@163.com

\* Correspondence: shisongfox@163.com; Tel.: +86-531-8861-7528

**Abstract:** In Huang-Huai-Hai plain of China, farmers collect the maize straw for livestock during maize harvest to increase their revenue. To maintain the sustainable productivity of the soil, all straw after the wheat harvest is returned to the field. This straw brings difficulties in the no-till seeding for maize after wheat harvest, and thus it is necessary to develop efficient no-till seeders that can cope with heavy residue and improve sowing quality. In this work, we designed a wide-strip-till no-till pneumatic maize (WNPM) seeder to satisfy the need in this plain. The key parameters of the opposite-placed anti-blocking mechanism of the WNPM seeder were determined via the discrete element method (DEM) technology, while the parameters of the pneumatic maize seed meter were specified using the coupled simulation of computational fluid dynamics (CFD) and DEM. We also carried out field experiment to test the performance of our machine. Under the operating speed of 8 km/h, the soil disturbance was 38.2%. Moreover, the straw cleaning rate achieved 94.4% in the seeding belt while the residue cover index of the seed plot was over 58%, and the seeding performance was improved significantly. The qualified seed spacing index, uniformity variation coefficient, qualified index of sowing depth and variation coefficient of sowing depth were 96.6%, 19.1%, 95.1% and 3.2%, respectively. In general, the WNPM seeder improves the working efficiency of maize sowing because both the reliable working speed and the sowing quality were increased. These results are of considerable importance for crop production in Huang-Huai-Hai plain of China.

**Keywords:** conservation tillage; no/minimum-till pneumatic seeder; anti-blocking; maize seed meter; maize precise sowing



**Citation:** Li, H.; Liu, H.; Zhou, J.; Wei, G.; Shi, S.; Zhang, X.; Zhang, R.; Zhu, H.; He, T. Development and First Results of a No-Till Pneumatic Seeder for Maize Precise Sowing in Huang-Huai-Hai Plain of China. *Agriculture* **2021**, *11*, 1023. <https://doi.org/10.3390/agriculture11101023>

Academic Editors: Massimo Cecchini and John M. Fielke

Received: 20 August 2021

Accepted: 15 October 2021

Published: 19 October 2021

**Publisher's Note:** MDPI stays neutral with regard to jurisdictional claims in published maps and institutional affiliations.



**Copyright:** © 2021 by the authors. Licensee MDPI, Basel, Switzerland. This article is an open access article distributed under the terms and conditions of the Creative Commons Attribution (CC BY) license (<https://creativecommons.org/licenses/by/4.0/>).

## 1. Introduction

The Huang-Huai-Hai Plain, with an area of  $3 \times 10^5$  km<sup>2</sup>, is located in the eastern part of China, ranging from 31°36' N to 40°29' N and 112°13' E to 120°53' E [1]. It covers many highly populated areas in five provinces (Hebei, Shandong, Henan, Anhui and Jiangsu) and two administrative cities (Beijing and Tianjin) [2]. It is the major crop-producing region in China. As an annual double-cropping plain (winter wheat and summer maize), successful crop production in this plain is one of the country's highest priorities. But the average maize yield here is  $5.89 \times 10^3$  kg/hm<sup>2</sup>, ranking only 21st in the world [3,4]. What is more serious is that this area is suffering from more frequent drought [5]. It has been demonstrated that conservation tillage (CT) can improve the water use efficiency, reduce wind and water erosion, increase yields of winter wheat and summer maize by 7–12%, and reduce costs by up to 20%, compared with the traditional tillage [6–10]. However, farmers in this area still collect the maize straw for livestock to increase their revenue. This

is only the straw after the wheat harvest is returned to the field in order to maintain the sustainable productivity of the soil. This returned heavy residue brings difficulties for the no-till seeding for maize after wheat harvest [11]. It is important to develop efficient no-till seeders that can cope with heavy residue.

Seeding at a low forward speed is one of the effective ways to ensure the sowing quality of the no-till seeders in the field covered with heavy residue. Before 2010, no-till sowing of maize after wheat harvest has been realized at a working speed of  $\leq 3$  km/h in the Huang-Huai-Hai Plain after several years of research. Several small–medium-sized no-till maize seeders (e.g., 2BMX-5 wheat-corn universal no-tillage planter, 2BMDF-2/7 row-followed no-till wheat and maize planter) were developed in CT soil environment [12–14]. The sowing quality and efficiency are limited due to the multi-purpose of sowing different crops and the poor seedbed conditions. Since then, many maize no-till planters have been developed, such as 2BMQ-180/3 no-tillage maize planter, 2BMQ-180/3 no-tillage maize planter and 2BQM-2 type maize ridge planter [15–17]. Moreover, a higher working speed of 3~6 km/h was realized by the above maize planters using different sorts of powered anti-blocking mechanisms, such as horizontal residue-throwing finger-wheel device [18], the drum-type anti-blocking mechanism [19], strip-chop cutter and stubble clean disk [20], active straw-removing anti-blocking device [21,22], and separating-guiding anti-blocking mechanism to move residue away from the seedbeds [23,24]. However, none of these studies discuss the performance of precision planting of maize, which can help to increase farmers' income [25].

Vacuum meter system has proven to be an excellent option for precision sowing with lower rate of seed damage caused by seed plate, and broader spectrum of applicability [26]. Vacuum seeders use 90% less seed and achieve higher working speed, which help the farmers by saving costs [27,28]. In U.S. and Sweden, John Deere no-till seeder and Vaderstad Tempo seeder, equipped with vacuum meter system, can work at a speed higher than 8 km/h on the large-scale farmland with light residue [29,30]. However, their working performance on the small-scale farmland with heavy residue is unknown. The existing of crop residues on the field surface decrease planting depth and uniformity, and increases the number of seeds placed closer to the surface [31,32]. Poor corn stand establishment, large variations in seed depth, and uneven emergence have been shown to decrease corn grain yield or, at least, to limit yield potential [33,34].

The qualities of residue handling and maize sowing for no-till seeders are prerequisite to achieve optimal plant density and successful crop production [35–37]. Since seeding is usually a very time-sensitive operation—with only a short period offering the right climatic conditions [38,39]—it is important to ensure the quality of maize planting under no-tillage practices with heavy residues at high working speed. In this paper, we report development and first results of a wide-strip-till no-till pneumatic maize (WNPM) seeder in Huang-Huai-Hai Plain of China, aiming at improving the working efficiency of maize sowing to overcome the problems caused by the heavy residue. We focused on the parameter design and performance testing of anti-blocking mechanism and maize seed meter of the WNPM seeder, which are relevant with the sowing quality in no-till conditions. The comparisons of different tillage systems or no-till machines are beyond the scope of this paper.

## 2. Design of the WNPM Seeder

### 2.1. Machine Structure and Working Principle

As shown in Figure 1a, considering the surface of the farmland was covered with wheat straw in double-cropping area of Huang-Huai-Hai Plain of China, the WNPM seeder was composed of opposite-placed anti-blocking mechanism, subsoiling device, powered rake device, multiple profiling devices' profiling mechanism, transmissions, and air suction seed-metering device, etc. This complete machine was 2.5 m wide and 2.6 m long with four sets of seeding units. To realize a superior seeding quality at higher working speed, the first step should be building suitable soil environment at no-tillage cropping system. As shown in Figure 1b, the opposite-placed anti-blocking mechanism chopped the straw at

high rotating speed and flipped the straw to the lateral of the straw area on both sides of the seed belt. The subsoiling device was schemed behind each anti-blocking mechanism to layer the fertilization deeply before sowing. The multiple profiling pressing devices were installed before and after sowing to ameliorate soil compactness. The roller flattened the seed beds before sowing. Subsequently, a neat seedbed was formed, whose characteristics played an important role in crop performance [23,40,41]. Finally, the developed air suction seed-metering device with driving and guiding auxiliary seed filling was adopted to realize precision seeding on the prepared seedbed.

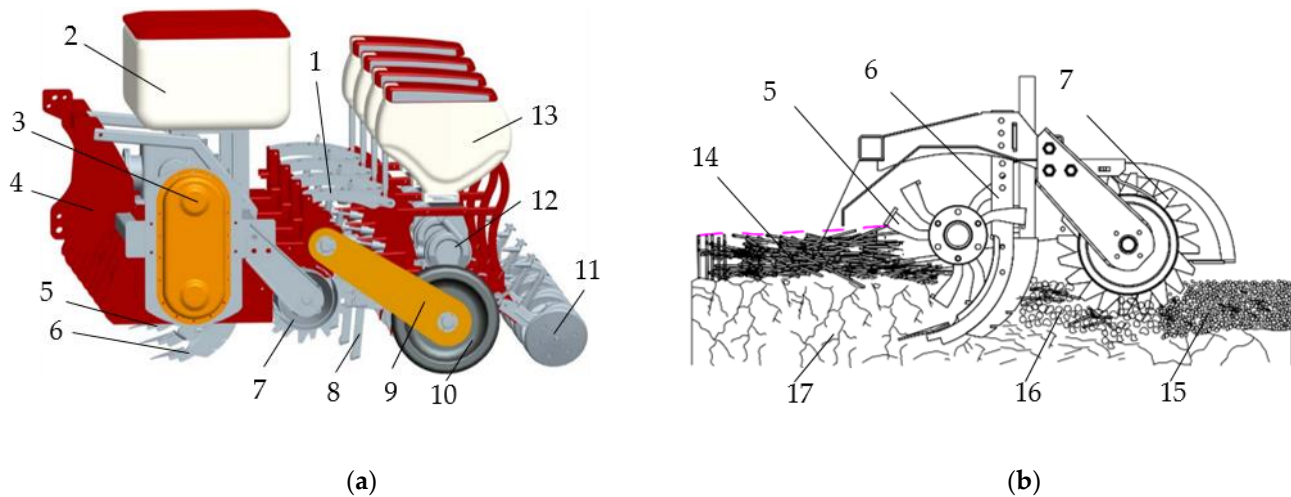


**Figure 1.** Structure and working principle of the WNPM seeder. (a) The overall structure of the WNPM seeder; (b) Method of seed bed preparation before sowing. Note: 1, Profiling mechanism; 2, Fertilizer box; 3, Side gearbox; 4, The frame; 5, Opposite-placed anti-blocking mechanism; 6, Subsoiling device; 7, Profiling and pressing device before sowing; 8, Ditching knife; 9, The support device of ground wheel; 10, The ground wheel; 11, Profiling and pressing device after sowing; 12, Air suction seed-metering device; 13, Seed box; 14, Farmland covered with straw; 15, Prepared seed bed before sowing; 16, Soil particle after subsoiling; 17, Hard soil before tillage.

## 2.2. The Opposite-Placed Anti-Blocking Mechanism

The opposite-placed anti-blocking mechanism, which was located in front of the subsoiling and fertilization device, was composed of three groups of left and right scimitars. According to the GB standards [42], the left and right of MIIT245 scimitars were selected for cutting the heavy residues. During the cutting process, the left and right machetes cut the straw and pulled it away from both sides of the subsoiling knife to form a seedling belt with relatively less straw. In the WNPM seeder, four sets of opposite-placed anti-blocking mechanism were used and were mounted on the same rotating shaft. As shown in Figure 2, the four anti-blocking mechanism units are centered on the shaft and symmetrically distributed. In particular,  $3 \times 2$  left and  $3 \times 2$  right scimitars were symmetrically distributed on the left-half and right-half shaft, respectively. Scimitars on each half shaft were arranged in three spiral lines. The helix angle  $\beta$  was  $30^\circ$  and the rising angle  $\lambda$  was  $60^\circ$  between two adjacent knives on the same spiral line in order to ensure the dynamic balance of anti-blocking device and straw side throwing.

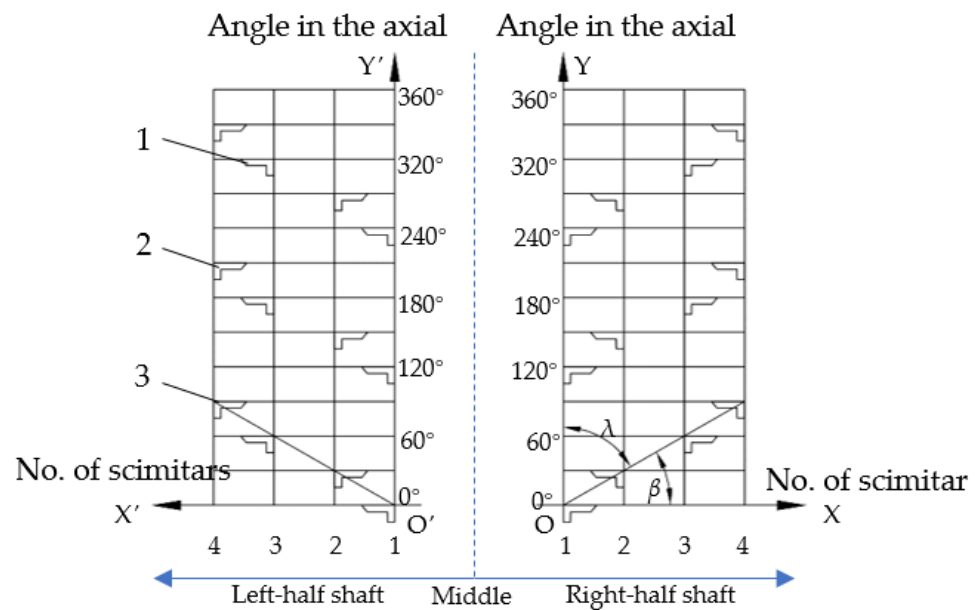


**Figure 2.** Schematic of axial scimitars' arrangement of the anti-blocking mechanisms. Note: 1, left scimitar of MIIT245 type; 2, right scimitar of MIIT245 type; 3, spiral line.

According to the agronomic requirements of planting in Huang-Huai-Hai Plain, the row spacing of sowing corn is 650 mm, and the row spacing of wheat sowing is 200 mm. As shown in Figure 3a, to prevent interference and ensure effective stubble removal, the spacing  $B_1$  between the left and right scimitars of the opposite-placed anti-blocking mechanism was as follows:

$$B < B_1 - 2b_1 + b_2 < B_2 \tag{1}$$

where  $b$  is the width of subsoiling shovel of chisel type (30 mm),  $b_1$  is the vertical length of MIIT245 scimitar (75 mm),  $b_2$  is the thickness of MIIT245 scimitar (10 mm),  $B_2$  is the row spacing of wheat stubble (200 mm). Meantime, the height of the anti-blocking device from the ground should meet the following formula during the operation:

$$H = R - h \tag{2}$$

where  $R$  is the radius of MIIT245 scimitar (245 mm),  $h$  is the penetration depth of the MIIT245 scimitar (mm). Since the soil depth is positively related to the stubble removal effects and negatively related to the power consumption [41], therefore, the penetration depth  $h$  was finally determined as 50 mm.

The rotating speed was also relevant with the working performances of the power consumption and the quality of straw cleaning of the seed belt [32]. The quality of crushing and scattering the straw was the premise to ensure high-speed sowing under no tillage. To realize the effective crushing of straw, the motion trajectory of the anti-blocking device should be cycloid [43]. As shown in Figure 3b, the formed trajectory of the cycloid when the MIIT245 scimitar of the opposite-placed anti-blocking mechanism was operating, was as follows:

$$\begin{cases} x = R\cos(\omega t) + vt \\ y = R\sin(\omega t) \end{cases} \tag{3}$$

where  $R$  is the turning radius of the scimitar (m),  $\omega$  is the angular velocity of the scimitar (rad/s),  $v$  is the implement forward speed (m/s),  $t$  is the movement time of cutter roller (s). Note that the rotating shaft of the anti-blocking mechanism is the origin of the coordinate system, the forward direction of the tractor is the positive direction of  $x$ -axis while the positive direction of  $y$ -axis is perpendicular to the field.

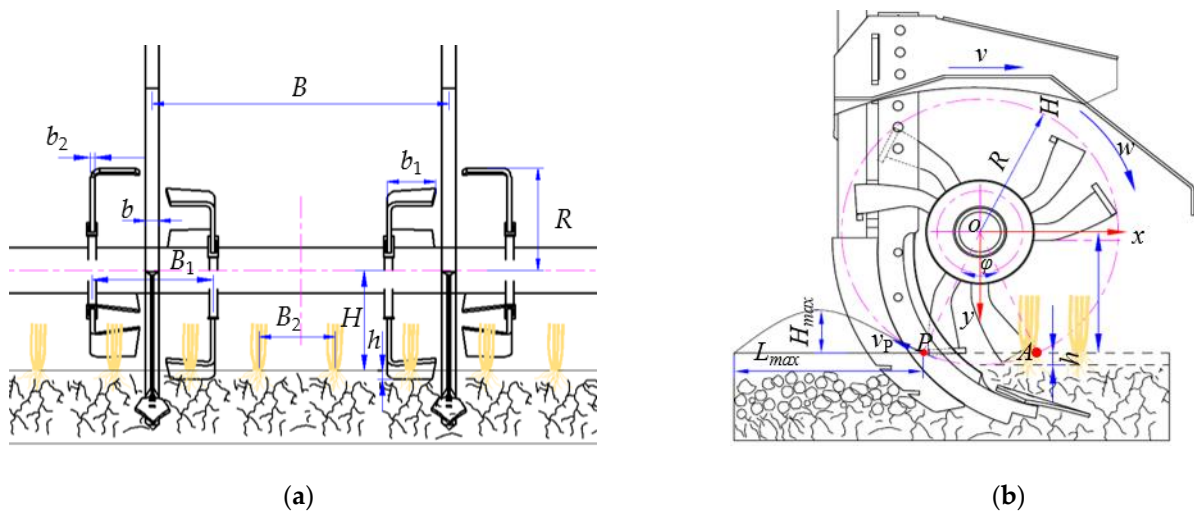


**Figure 3.** The working mechanism and parameter design of straw crushing and throwing. (a) Relative position of the opposite-placed anti-blocking mechanism; (b) Working principle diagram of the anti-blocking device.

The horizontal partial velocity  $v_x$  and vertical partial velocity  $v_y$  could be obtained by differentiation of the Formula (3); they were calculated as follows:

$$\begin{cases} v_x = v - R\omega \sin(\omega t) \\ v_y = R\omega \cos(\omega t) \end{cases} \quad (4)$$

Since the straw would be pushed forward when the horizontal partial velocity  $v_x \geq 0$ , the  $v_x$  must be backward to prevent the seeder from blocking. Furthermore, the absolute linear speed of the scimitar should not be lower than the required stubble cleaning speed. To chop the straw and residues effectively, there was a relationship between the absolute linear speed and the stubble cleaning speed, as follows at the point A:

$$n \geq 30(v_c + v) / [\pi(R - h)] \quad (5)$$

$$\lambda = R\omega / v \quad (6)$$

where  $n$  is the rotation speed of the scimitar (r/min),  $h$  is the penetration depth of the scimitar (m),  $v_c$  is the required stubble cleaning speed (m/s),  $v$  is the forward speed of the WNPM seeder (m/s),  $\lambda$  is the speed ratio between the rotary linear speed of the scimitar and the forward speed of the WNPM seeder.

To ensure the maize sowing quality under no-tillage conditions with the forward speed of  $\geq 8$  km/h (i.e.,  $v$  should be  $\geq 2.2$  m/s), the required stubble cleaning speed  $v_c$  was determined to be 7.5 m/s [44,45]. Since  $R = 0.245$  m,  $h = 0.05$  m, the rotation speed  $n$  was  $\geq 475$  r/min according to the above formula, and the speed ratio  $\lambda \geq 5.54$  concurrently. Furthermore, at the point P, where scimitars would leave the field at the next moment, the straw would be chopped and thrown. Obviously, the horizontal distance  $x_p$  and vertical distance  $y_p$  of the thrown straw was matched by the following formulas, respectively:

$$\begin{cases} x_p = x_{p0} - v_p t \cos \frac{\varphi}{2} \\ y_p = y_{p0} + \frac{1}{2} g t^2 - v_p t \sin \frac{\varphi}{2} \end{cases} \quad (7)$$

where  $\varphi$  is the tiller angle of the scimitars,  $v_p$  is the linear velocity of point P (m/s),  $H$  is the height of the anti-blocking device from the ground (m),  $x_{p0}$  and  $y_{p0}$  are the horizontal and vertical coordinates at the initial position of the chopped straw, respectively (m). Here,  $\varphi = 2 \arccos H / R = 74.5^\circ$ ,  $v_p = 2\pi n R$ .

The maximum distance  $L_{\max}$ , when straw was thrown in the x-axis direction, and the maximum height  $H_{\max}$ , when the straw was thrown in the y-axis direction, were as follows, respectively:

$$\begin{cases} L_{\max} = \frac{v_p^2 \sin \varphi}{2g} \\ H_{\max} = \frac{v_p^2 (1 - \cos \varphi)}{4g} \end{cases} \quad (8)$$

### 2.3. The Design of Maize Seed Meter

Seed meter with reliable working performance was an important guarantee for realizing no-till sowing with high efficiency and high quality. To control the movements of seeds in the seed meter was the first step to deliver the seeds from seed disc to tube flighted belt and on to the seed trench. The pneumatic maize seed meter was designed and used on the WNPM seeder. As shown in Figure 4, the pneumatic maize seed meter was composed of air duct with positive pressure, air duct with negative pressure, steering engine, exhaust port, flow-divider valve, air nozzle, seed guided groove of seed disc, seed cleaning device, seed disc, drive motor, etc. The motor and steering engine cooperated to control the speed of the seed disc and the angle of the diverter valve simultaneously, to realize the precise seeding. The movements of seeds in the seed meter consisted of being adsorbed, being separated, singulation, and being dropped. At the seed adsorbing progress, a pressure difference was formed on both sides of the seed disc by connecting the negative pressure air pipe to the fan, so that the shaped holes generated suction to adsorb seeds. Subsequently, special shaped hole guide grooves were designed on the seed disc to separate seed from the seed population by driving, collision, and guiding the seeds. Then, at the singulation progress, a single seed was left on the shaped hole by repeated interactions with the internal and external seed cleaning knives. At last procedure, the seeds fell into the seed bed through the seed guide tube under the action of self-weight.

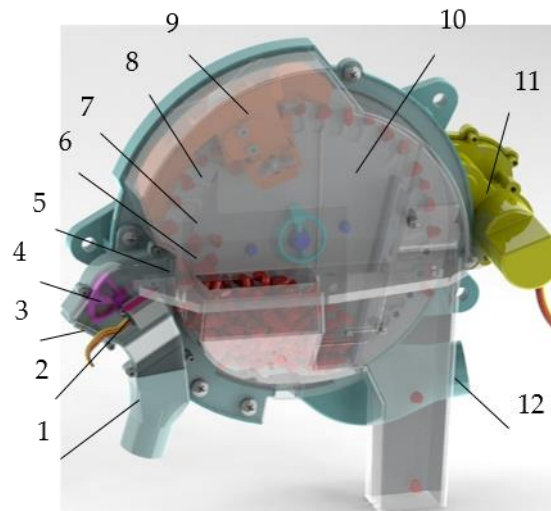


**Figure 4.** Structural figure of the pneumatic maize seed meter. Note: 1, air duct in positive pressure type; 2, steering engine; 3, exhaust port; 4, flow-divider valve; 5, air nozzle; 6, maize; 7, the upper cover of seed meter; 8, seed guided groove of seed disc; 9, seed cleaning device; 10, seed disc; 11, drive motor; 12, air duct in negative pressure type.

Appropriate meter disc provided positive load-in and hold of the seed for precise handoff to the delivery tube [46]. As a key part of the meter disc, the curved seed guided groove of the meter disc not only guided the seed moving toward the hole actively, but also improved the loose degree of the population and reduced the resistance of seed removal. All of these features are important for better sowing quality. As shown in Figure 5, the seed and the seed guide groove were contacted at point  $O'$  on the disc in the initial state. After a

period of  $t_1$ , the seed disc rotated angle  $\varphi_1$  and the point  $O'$  moved to point  $A$ . Meanwhile, the seed moved along the seed guide groove curve from point  $O'$  to point  $A_1$ . During this progress, the seed-metering disc moved in a circle at constant speed, while the seed moved straight at a variable acceleration speed. As indicated in researches [37,46], the relative motion track of the seed was also the seed guided groove curve. In order to drive the seed into the air-forced control area of the seed holes, it could be described as follows:

$$\begin{cases} x_{A_1} = R_1 [\cos\varphi_1 + \gamma^{-1} \cdot \tan(\gamma \cdot \varphi_1) \sin\varphi_1] \\ y_{A_1} = R_1 [\sin\varphi_1 - \gamma^{-1} \cdot \tan(\gamma \cdot \varphi_1) \cos\varphi_1] \end{cases} \quad (\varphi_1 \in (0, \xi)) \quad (9)$$

where  $x_{A_1}$  is the X-axis coordinate value of point  $A_1$  in the absolute XOY coordinate system (m),  $y_{A_1}$  is the Y-axis coordinate value of point  $A_1$  in the absolute XOY coordinate system (m),  $R_1$  is the radius of the base circle of seed guide groove curve (m),  $\varphi_1$  is the rotation angle of the seed disc after a period of  $t_1$  ( $^\circ$ ),  $\xi$  is the upper limit of angle  $\varphi_1$  ( $^\circ$ ),  $\gamma$  is the curvature coefficient of seed guide groove, and value ranged from 0.01 to 0.99.

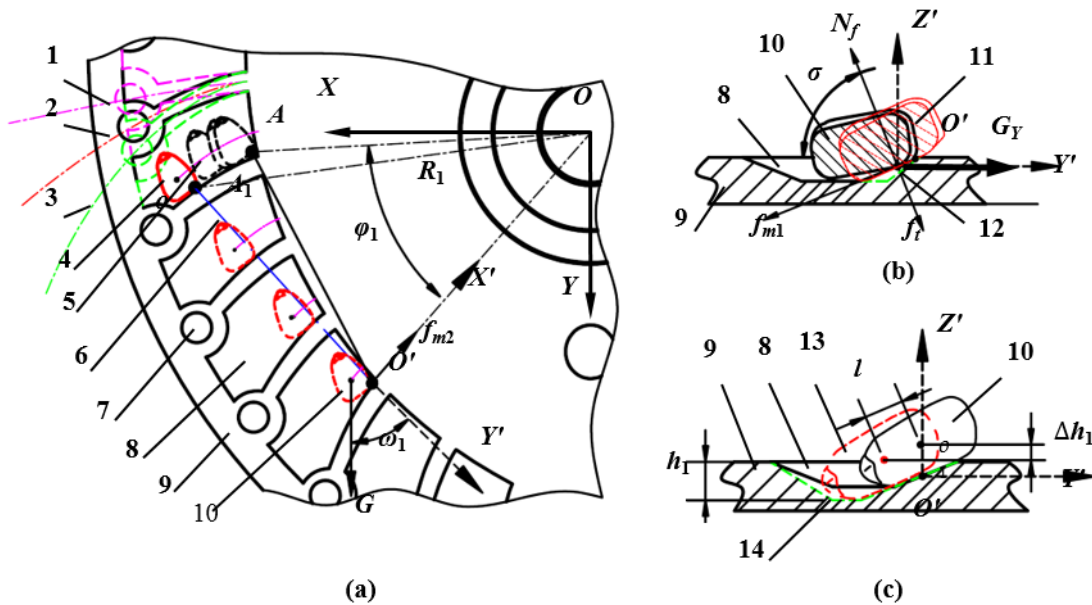


**Figure 5.** Key parameter design of the pneumatic maize seed meter. (a) Curvature coefficient of seed guide groove curve; (b) Inclined angle of the seed guide groove; (c) Depth of the seed guide groove. Note: 1, Seed guide groove curve when  $\gamma = 0.9$ ; 2, seed guide groove curve when  $\gamma = 0.5$ ; 3, seed guide groove curve when  $\gamma = 0.1$ ; 4, target seed after moving; 5, relative trajectory of seed; 6, absolute trajectory of seed; 7, shaped hole; 8, seed guided groove; 9, seed-metering plate; 10, target seed before moving; 11, seed in seed guide groove with small inclined angle; 12, inclined surface of seed guide groove; 13, seed in deeper seed guide groove; 14, deeper seed guide groove; XOY is absolute coordinate system while  $X'O'Y'$  is the relative coordinate system.

At the working process, when the disc rotated the angle  $\varphi_1$ , the curvature coefficient  $\gamma$  of seed guide groove determined the distance of the moved seed from the shaped hole along the normal direction, and the contacted area between the seed and the seed disc of the seed guide groove. The value of  $\gamma$  was negatively related to the hole length, i.e., when  $\gamma$  was larger, the hole length would be shorter, which would guide the seed entering the air-flow controlling area faster during seed adsorbing progress. However, the time of separating seed from the seed population would be shorter during the seeding progress of being separated and singulation. In addition, the seed could move in the seed guided groove if the resultant force on the X' axis was negative on the  $X'O'Y'$  plane. The direction of the resultant force along the inclined plane of the seed guide groove was consistent with

the friction  $f_{m1}$  on the  $O'Y'X'$  plane (shown as Figure 3b,c). Therefore,  $f_{m1}$  and  $f_{m2}$  were calculated as below:

$$\begin{cases} f_{m2} \leq G \sin \omega_1 \\ f_{m1} \geq G_Y \sin \sigma \end{cases} \quad (10)$$

Here  $N_f = f_t + \cos \sigma$ ,  $f_{m1} = f_{m2} = N\mu$ ,  $G_Y = G \cos \omega_1$ .

After simplification, the Formula (10) could be as follows:

$$\begin{cases} \frac{f_t \cdot \mu}{\sin \omega_1 - \mu \cos \omega_1 \cos \sigma} \leq G \\ \frac{f_t \cdot \mu}{\cos \omega_1 (\sin \sigma - \mu \cos \sigma)} \geq G \end{cases} \quad (11)$$

where  $N_f$  is the upward support force of the inclined surface of seed guide groove (N),  $f_t$  is the resistance to remove a single seed from the seed population during the separating progress (N),  $f_{m1}$  is the friction along the inclined surface of seed guide groove (N),  $f_{m2}$  is the friction along the  $X'$  axis (N),  $G$  is the gravity of maize seed (N),  $G_Y$  is the component of seed gravity on  $Y'$  axis,  $\omega_1$  is the inclination between gravity and  $Y'$  axis ( $^\circ$ ),  $\sigma$  is the slope angle of the seed guide groove ( $^\circ$ ),  $\mu$  is the sliding friction coefficient between seed and seed disc. This indicated that, when  $\sigma$  was smaller, the seed was apt to make absolute movement along the tangent of the base circle. At the same time, the depth  $h_1$  of seed guided groove and the contact area of the seed on the inclined surface of the groove showed a positive relationship significantly, and was calculated as below:

$$\Delta s = B_p \cdot l = B_p \cdot \Delta h_1 \cdot \cos \sigma \quad (12)$$

where  $B_p$  is the average width of seeds (m),  $l$  is the distance between centroids before and after seed movement (m),  $\Delta h_1$  is the sinking depth of seed guide groove (m). The movement of seed which was guided by the seed guided groove would become more stable as the contact area increased by increasing  $h_1$  and decreasing  $\sigma$ , however, seed adsorbing progress would be affected through severe disturbance of the seed population.

### 3. Optimization of Multi-Parameter through DEM Simulation by EDEM

The Discrete Element Method (DEM), also called Discrete Element Modeling, is a numerical technique to model the motion of an assembly of particles which interact with each other through collisions. It was originally developed by Cundall and Strack [47] for predicting the behavior of soil grains and belongs to the group of "Particle Based Simulations". In recent years, computational modeling based on DEM has been widely utilized in agricultural progresses [48]. González-Montellano et al. [49] used the DEM to simulate grain flow in silos. The DEM was also utilized for the simulation of grain–straw separation [50], fertilizer spreading [51], and soil-mechanism interaction [52], etc.

More particularly, DEM was a superior design method for metering devices by coupling with the method of Computational Fluid Dynamics (CFD). Han et al. [53] used the DEM-CFD coupling approach for optimization of an inside-filling air-blowing maize precision seed-metering device. Lei et al. [54] simulated the seed motion in seed feeding device with DEM-CFD coupling approach for rapeseed and wheat. Those results proved the DEM-CFD coupling approach to be a reliable instrument for simulating the physical phenomenon of seed movement in the air-flow field. In this part, we used the DEM method and DEM-CFD coupling approach for optimization of the key parameters of opposite-placed anti-blocking mechanism and pneumatic maize seed meter, respectively.

#### 3.1. Parameter Selection of the Opposite-Placed Anti-Blocking Mechanism

##### 3.1.1. Materials and Methods of the DEM Simulation of the Anti-Blocking Mechanism

The abilities of residue handling were proved to be the most significant factor for the creation of suitable soil environment [36]. Key parameters of the anti-blocking mechanism were optimized by establishing relationships between the parameters and their performances. The distance between the left and right machetes, the rotating speed of

the cutter shaft, and the forward speed of the anti-blocking mechanism were considered to be the most important factors affecting the effect of straw treatment in this research. Meanwhile, the residue handling performances were investigated, which included the rate of straw cleaning, the average displacement of straw moving, and the stress of the anti-blocking mechanism afforded. Since the DEM has been proved to be an effective method to predict the working performance for the soil-straw-tool interaction [55,56], all the above performances were obtained through simulating the working progress of the opposite-placed anti-blocking mechanism on the heavy straw-covered field by using EDEM software, which is an application software of using Discrete Element Method.

Proper prediction of this interaction using EDEM depends upon the model parameters [57]. The key parameters of the soil and wheat straw were shown in Table 1. Furthermore, the soil and straw were taken from the long-term fixed trial field in Jinan and Dezhou city, which are both located in the Huang-Huai-Hai Plain. The authors have already illustrated the relative test methods in former research, as Reference [24]. Then, a simplified model of soil trough was established with the size of 2000 mm (length)  $\times$  1000 mm (width)  $\times$  500 mm (height) according to the requirements of simulation test. The particle radius of soil was 4 mm, the crushed straw model was a long linear model with the length of 90 mm composed by spherical balls whose radius was 5 mm and the distance between ball center was 5 mm. To simulate the interaction among the machine, soil and straws, Hertz-Mindlin (no slip) + bonding model has been widely used by Yao et al. [22], Niu et al. [24] and Jiang et al. [58]. All the researches were conducted in Huang-Huai-Hai Plain, and moreover, stated the positive results by using the Hertz-Mindlin (no slip) + bonding model to simulate the real work conditions. Thus, the Hertz-Mindlin (no slip) + bonding model was also used here. As other researches indicated [59,60], the contacting models of soil, straw and geometry were established to endure the displacement from tangential and normal. The bonding among contacting model would not be damaged until the shear stresses from the normal and tangential direction reached the maximum. The environment of the soil surface which was fully covered with straw after wheat harvest was simulated by 25,000 soil particle models and 4000 straw particle models.

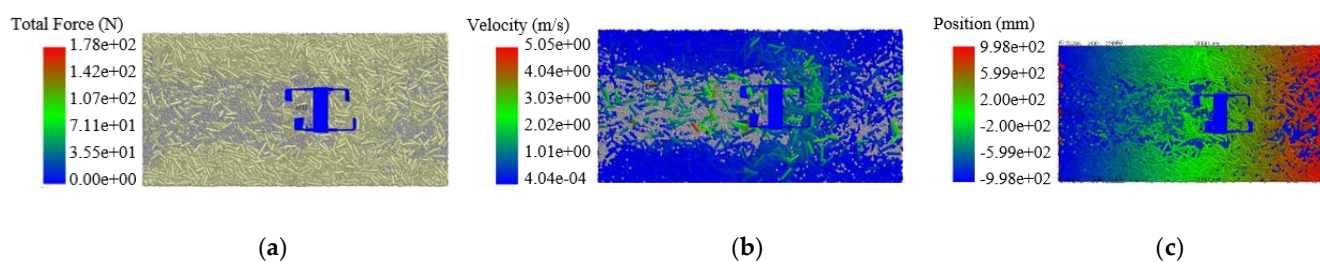
**Table 1.** Parameter settings for EDEM simulation.

Parameters	Value	Parameters	Value
Soil density $\rho$ /(kg·m <sup>-3</sup> )	1850	Soil shear modulus $G$ /Mpa	1
Poisson's ratio of soil $\nu$	0.35	Static friction coefficient among soil $\mu_s$	0.541
Straw density $\rho_1$ /(kg·m <sup>-3</sup> )	241	Shear modulus of straw $G_1$ /Mpa	1
Poisson's ratio of straw $\nu_1$	0.4	Static friction coefficient between straws $\mu_{s1}$	0.3
Iron density $\rho_2$ /(kg·m <sup>-3</sup> )	7865	Shear modulus of iron $G_2$ /Mpa	$7.9 \times 10^4$
Poisson's ratio of straw iron $\nu_2$	0.3	Static friction coefficient between soil and iron $\mu_{s2}$	0.6
Recovery coefficient among soil $e$	0.6	Recovery coefficient among straw $e_1$	0.3
Recovery coefficient between soil and iron $e_2$	0.6	Recovery coefficient between straw and iron $e_3$	0.3
Rolling friction coefficient among soil $\mu_r$	0.31	Rolling friction coefficient among straw $\mu_{r1}$	0.02
Rolling friction coefficient between soil and iron $\mu_{r2}$	0.6	Rolling friction coefficient between straw and iron $\mu_{r3}$	0.3

As shown in Table 2, the orthogonal design with three factors (i.e., distance between the opposite-placed rotary tiller, rotating speed, forward speed) and three levels was established in EDEM separately. The penetration depth of the anti-blocking mechanism was 50 mm. During the simulation (Figure 6a,b), the soil trough was divided into 100 grids with 10 grids along the Y direction and the 10 grids along the X direction (Figure 6c). Then, the number of straws in the grid, which was cultivated by the machine, was counted before and after the anti-blocking mechanism passing through the grid, and the straw cleaning rate was calculated. Meanwhile, the average straw displacement and the force of the anti-blocking mechanism afforded were obtained after simulation by using EDEM post processing module, EDEM Analyst.

**Table 2.** Parameter settings for EDEM simulation of opposite-placed anti-blocking mechanism.

Level	Factors		
	Distance between the Left and Right Machetes $B_1$ (mm)	Rotating Speed of the Cutter Shaft $n$ (r·min <sup>-1</sup> )	Forward Speed $v$ (km·h <sup>-1</sup> )
1	200	300	7
2	260	500	8
3	320	700	9

**Figure 6.** Simulation diagrams of the opposite-placed anti-blocking mechanism. (a) The force of the anti-blocking mechanism afforded; (b) Straw movement; (c) Straw displacement.

### 3.1.2. Data Analysis

Mean values were calculated for each of the variables, and ANOVA was used to assess the factor effects on the measured variables by the least significant difference (l.s.d.) method. In all analyses, a probability of error smaller than 5% ( $p = 0.05$ ) was considered statistically significant. The SPSS analytical software package (13.0) was used for all the statistical analyses.

### 3.1.3. Simulation Results and Discussion of the Opposite-Placed Anti-Blocking Mechanism

As shown in Table 3, the results were obtained through the orthogonal test. The average straw cleaning rates at three different (300 r/min, 500 r/min, 700 r/min) rotating speed levers were 84.0%, 93.3%, 90.6%, respectively, while the straw displacements were 612.4 mm, 688.7 mm, 1045.4 mm, respectively. Furthermore, the mean afforded force of the anti-blocking mechanism at 300 r/min, 500 r/min and 700 r/min rotating speed levers were 359.4 N, 495.0 N and 669.8 N, respectively. The results indicated that the rotating speed had significant effects on straw cleaning rate, straw average displacement, and afforded force of the anti-blocking mechanism, which was consistent with the results of Fang [60]. However, the differences of above three working performances at different distance and forward speed levels were almost negligible, but the distance between the opposite-placed tillers affected the straw cleaning rate significantly. Specifically, the average straw cleaning rates at 200 mm, 260 mm, 320 mm spacing of the anti-blocking mechanism were 92.6%, 92.2%, 87.1%, respectively.

Yao et al. [22], Siemens et al. [23], Niu et al. [24], Fang [60] and Fang et al. [61] proved that the simulation results of straw cleaning rate, straw displacement, and afforded force were consistent with the results of soil tank or field experiments for testing the interactions among the anti-blocking mechanism, soil and straw. In this paper, the parameters of anti-blocking mechanism were selected according to the simulation results of the orthogonal tests. As researches illustrated [59,60], the higher the rotating speed was, the greater was the straw cleaning rate and the power consumption. Since the forward speed had no significant effect on the working performance at the forward speed of 7–9 km/h, the rotation speed of anti-blocking mechanism was determined as 500 r/min finally. Furthermore, the distance of the opposite-placed blades was determined as 260 mm at the working speed of 8 km/h. The speed ratio  $\lambda$ , tiller angle  $\varphi$ , maximum distance  $L_{\max}$ , and maximum height  $H_{\max}$  were then calculated to be 5.83, 74.5°, 8.1 m and 2.92 m, respectively, from the

Equations (6)–(8). The maximum displacement was obviously higher than the simulated value, which illustrated that the air resistance and the soil-buried straw after crushing should be reasonably considered.

**Table 3.** Results of the EDEM simulation. Note: Values within a column followed by the same letters are not significantly different at  $p = 0.05$ .

Order Number	Factors			Straw Cleaning Rate/%	Average Displacement of Straw/mm	Anti-Blocking Mechanism Afforded FORCE/N
	Distance of Machetes	Rotating Speed	Forward Speed			
1	1	1	1	85.9 a	602.4 a	323.9 a
2	1	2	2	96.3 b	698.1 b	466.1 b
3	1	3	3	95.6 bc	957.3 c	685.9 c
4	2	1	2	84.3 a	617.1 a	359.3 a
5	2	2	3	94.8 bc	613.9 a	501.6 b
6	2	3	1	97.5 c	1123.5 c	679.5 c
7	3	1	3	81.7 a	617.9 a	394.9 a
8	3	2	1	88.9 ab	754.1 b	517.2 b
9	3	3	2	90.8 ab	1055.3 c	643.9 c

### 3.2. Parameter Selection of the Pneumatic Maize Seed Meter

#### 3.2.1. Materials and Methods of the Seed Meter Simulation by DEM-CFD

According to the determinacy tracking model of the grain model [25,62], the simulation method of coupling DEM-CFD was used to assess the seeding performances of the pneumatic maize seed meter under a multiple group of parameters by using two-way EDEM-CFD software. During the coupled gas-solid EDEM-CFD simulation, particular multiphase coupling interface file (version 2.0) and the calculation method of the flow of pressure gradient force were introduced. The compilation and calling process of the pressure gradient force to the gas-solid coupling interface file is shown in Figure 7. First, the memory space of the pressure gradient force information was activated. Then, invoking of the flow-field information by using the secondary developed program UDF was followed. Finally, EDEM API, a program for compiling the particle custom attributes was used for extraction and analysis of the pressure gradient force information.

To achieve precise singulation and seed spacing regardless of seed size or shape, three kinds of common maize varieties (Denghai 605, Denghai 615 and Nonghua 101) in Huang-Huai-Hai area were collected to construct the 3D models. As shown in Figure 8, the maize seeds were scanned to obtain 3D point cloud data by reverse processing, and then fitted as solid model and bonded by multiple small particles by using the particle replacement method. The radius of the curve base circle of seed disc  $R_1$  and the number of shaped holes were designed as 160 mm and 34, respectively, according to the size of different maize varieties.

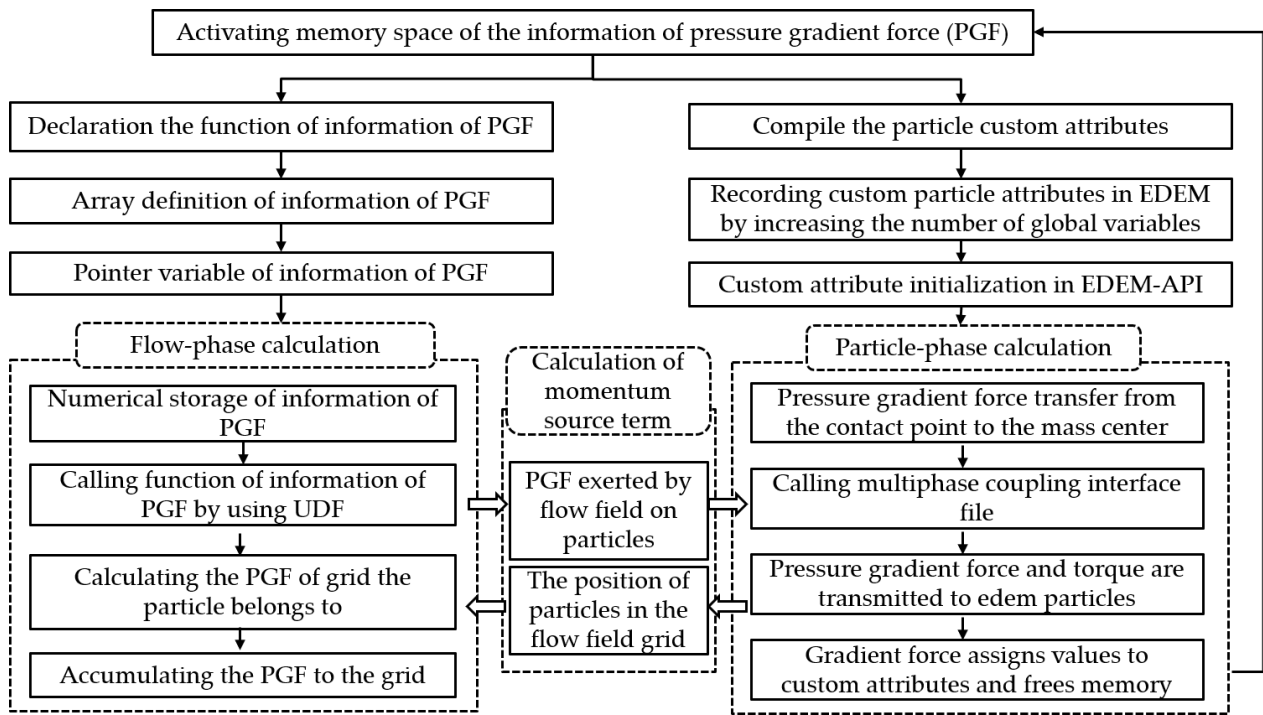


Figure 7. Diagram of compiling and transferring the pressure gradient force (PGF) during the EDEM-CFD simulation.

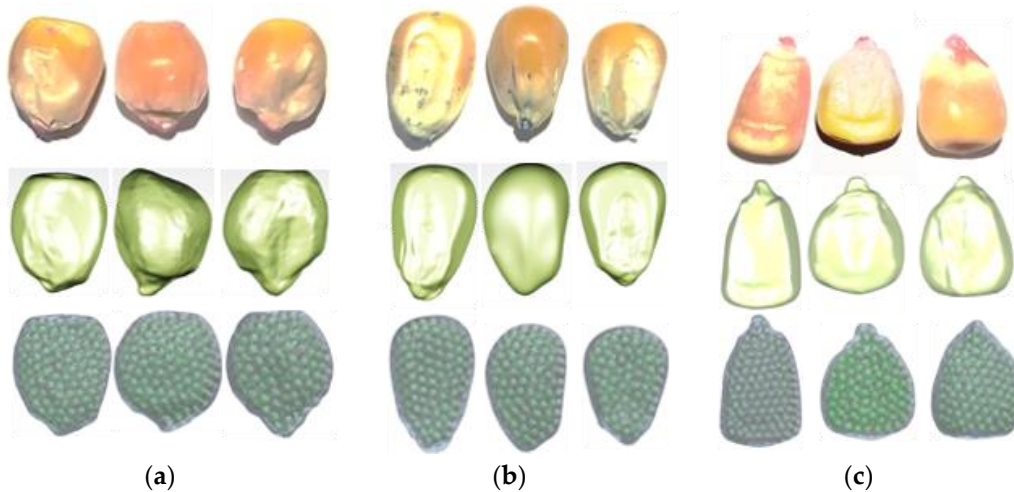
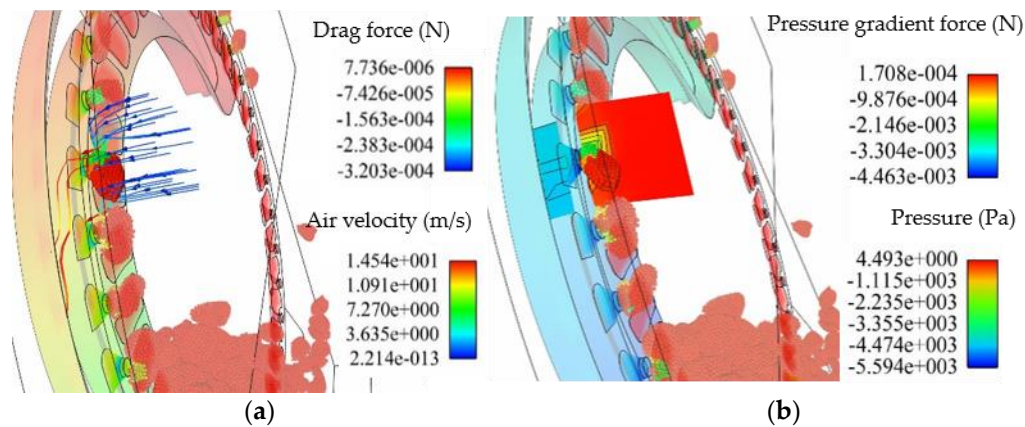


Figure 8. Simulation models of the maize seeds. (a) Denghai 605 variety; (b) Denghai 615 variety; (c) Nonghua 101 variety.

According to the working characteristics of the pneumatic maize seed meter, the particle field and air-flow field models for simulation calculation were established respectively (Figure 9). In order to complete the data exchange between the negative pressure chamber and the seed storage chamber under the rotating movement of the seed-metering disc, the grid of the seed-metering plate and seed guide groove were set as a moving grid by sliding grid method. The interfaces between the seed guide groove and the seed storage chamber, and the interfaces between the profile hole and the negative pressure airway were defined as the contact surface.



**Figure 9.** Coupled gas-solid EDEM-CFD simulation of the maize seed meter. (a) Drag force of the seeds afforded in the flow; (b) Gradient force of the seeds afforded under the pressure.

As shown in Table 4, the seed-metering plate and seed cleaning knife were made of polyhexamethylene hexanediamine (nylon 66), and the upper shell was made of methyl methacrylate polymer (acrylic). The contact parameters between particles, parameter between particles and geometry were determined by parameter calibration. In order to ensure the sowing quality of planter when the forward speed was 8.0 km/h, the rotation speed of seed-metering plate was set to be 2.0 rad/s (corresponding to plant spacing of 0.25 m, forward speed of 8.0 km/h), and the pressure of air intake was  $-5.5$  Kpa; 100 seed models were selected from each seed variety, thus the number of maize seed particles was 300. After particle replacement and bonding, the total number of particles was  $1.13 \times 10^5$ .

**Table 4.** Parameter settings for EDEM-CFD simulation of the maize seed meter.

Materials	Parameters					
	Poisson's Ratio	Shear Modulus/Pa	Density/(g·cm <sup>-3</sup> )	Collision Recovery Factor (with Particles)	Static Friction Coefficient (with Particles)	Rolling Friction Coefficient (with particles)
Maize	0.40	$1.37 \times 10^8$	2.25	0.19	0.03	0.002
Nilon66	0.28	$3.2 \times 10^9$	1.14	0.73	0.44	0.087
Acrylic	0.50	$1.77 \times 10^8$	1.18	0.71	0.46	0.093

During the EDEM-CFD simulation, the orthogonal design method was also used. The curvature coefficient  $\gamma$ , depth  $h_1$  and inclined angle  $\sigma$  of the seed guide groove of the seed-metering plate were taken as the test factors to optimize the seed guide groove of the seed disc. The seed filling process was usually divided into adsorption, separating and singulation, and dropping stages [25,46]. For each combined test, the above three stages were completed by artificial separation from the starting point to the ending point. Furthermore, the duration of adsorption process  $T_D$ , removal resistance in separating and singulation process  $F_R$ , and void fraction in dropping progress  $\delta_V$  were calculated in all the combined tests. The average value of the data was collected from 25 consecutive holes in each test. Moreover, the corresponding structural parameters of seed disc were optimized with the assessment indicators of  $T_D$ ,  $F_R$  and  $\delta_V$ .

### 3.2.2. Simulation Results and Discussion

ANOVA was used to assess the effects of different factors on the measured indicators by the least significant difference (L.S.D.) method. As the results in Table 5, the curvature coefficient  $\gamma$  and inclined angle  $\sigma$  of the seed guide groove had significant effects on the duration of the adsorption stage, the removal resistance during separating and singulation

process, respectively. The average duration of adsorption process at three different curvature coefficient levels (0.1, 0.5, 0.9) were 0.116 s, 0.112 s, 0.095 s, respectively. Furthermore, the mean removal resistance of the seed meter at 0°, 25° and 50° of the inclined angles were 0.0102 N, 0.0099 N and 0.0140 N, respectively. The results also showed that the duration  $T_D$  was significantly ( $p < 0.05$ ) affected by curvature coefficient  $\gamma$ . Meanwhile, the removal resistance  $F_R$  was affected by the inclined angle  $\sigma$  significantly ( $p < 0.05$ ). The influences of the three factors on void fraction  $\delta_V$  were  $\gamma > h_1 > \sigma$ . All the above results were almost agreed with Shi et al. [46]. Through the regression analysis, the three indicators were evaluated by the three factors as follows:

$$\begin{cases} T_D = 0.122 + 2.3 \times 10^{-5}\sigma - 0.002h_1 - 0.026\gamma & R^2 = 0.703 \\ F_R = 0.009 + 7.53 \times 10^{-5}\sigma^2 + 0.002\gamma & R^2 = 0.789 \\ \delta_V = 65 - 1.21\gamma + 0.54h_1 + 0.57\sigma - 0.72\gamma h_1 + 0.78\gamma\sigma - 2.03\gamma^2 - 1.62h_1^2 - 1.54\sigma^2 \end{cases} \quad (13)$$

Table 5. Simulation results of the maize seed meter.

Order Number	Inclined Angle $\sigma$ (°)	Depth of the Seed Guide Groove $h_1$ (mm)	Coefficient of Curvature $\gamma$	Duration (s)	Removal Resistance (N)	Void Fraction (%)
1	0	3	0.1	$1.06 \times 10^{-1}$	$8.70 \times 10^{-3}$	61.58
2	0	1.6	0.5	$1.19 \times 10^{-1}$	$9.90 \times 10^{-3}$	64.46
3	0	0.2	0.9	$9.75 \times 10^{-2}$	$1.21 \times 10^{-2}$	63.83
4	25	3	0.5	$1.08 \times 10^{-1}$	$8.90 \times 10^{-3}$	67.37
5	25	1.6	0.9	$9.20 \times 10^{-2}$	$1.08 \times 10^{-2}$	59.62
6	25	0.2	0.1	$1.19 \times 10^{-1}$	$1.00 \times 10^{-2}$	64.46
7	50	3	0.9	$9.60 \times 10^{-2}$	$1.41 \times 10^{-2}$	61.34
8	50	1.6	0.1	$1.22 \times 10^{-1}$	$1.35 \times 10^{-2}$	64.43
9	50	0.2	0.5	$1.08 \times 10^{-1}$	$1.43 \times 10^{-2}$	62.03

Relative researches [46,63] have indicated that, the higher of  $T_D$ , the smaller of  $F_R$  and the lower of  $\delta_V$ , contributed to the better working performance of the seed-metering device under the same working conditions. As above results illustrated,  $T_D$ ,  $F_R$  and  $\delta_V$  were all affected by the key parameters of the seed-metering disc. In order to obtain the best structural parameters of seed guide groove of seed-metering disc, the optimization module [64] was used to carry out multi-objective optimization analysis with higher adsorption duration, smaller seed removal resistance, and lower hole local porosity as the optimization objectives. The objective function and constraint conditions were as below:

$$\begin{cases} \max T_D(\gamma, h_1, \sigma) \\ \min F_R(\gamma, h_1, \sigma) \\ \min \delta_V(\gamma, h_1, \sigma) \\ s. t. \begin{cases} 0.1 \leq \gamma \leq 0.9 \\ 0.2 \text{ mm} \leq h_1 \leq 3.0 \text{ mm} \\ 0^\circ \leq \sigma \leq 50^\circ \end{cases} \end{cases} \quad (14)$$

After multi-objective optimization analysis, the curvature coefficient  $\gamma$  was determined to be 0.35, depth  $h_1$  and inclined angle  $\sigma$  were designed as 2.6 mm and 20.5°, respectively.

#### 4. Materials and Methods of Field Experiment

##### 4.1. Site Description

Field trials were conducted at Qihe region (36°48' N, 116°44' E) in Northwest Shandong in middle June of 2020, which is located in Huang-Huai-Hai Plain of China. The average annual temperature there is 12.9 °C with 212 frost-free days. Double cropping of winter wheat and summer maize is the main cropping system practiced in this region. Summer maize was usually seeded in early June. According to the USDA texture classification system, the soil at the station is a silt loam with bulk density of 1.33 g/cm<sup>3</sup>, pH of

8.0, soil moisture of 16.3%, and soil penetration of 2.4 MPa in the top 30 cm soil layer. As shown in Figure 10, the straw was crushed and returned to the field after the wheat was harvested in early June. The height of the straw stubble was 20 cm. The straw coverage was 1.15 kg/m<sup>2</sup> and the moisture content of the straw was 15.9%.



**Figure 10.** Experiment field covered with wheat straw before maize sowing.

#### 4.2. Field Test Contents and Methods

The wide seedling strip maize no-till pneumatic seeder was equipped with the Foton Lovol TG1654 Tractor, and worked at 8 km/h in the field test. The maize variety ‘Denghai 605’ was used in this test. As shown in Figure 11, the seeding rate and quality for the no-till seeder were calibrated following the China National Standards GB/T 20865–2017 “no/less tillage fertilization planter” [65] and GB/T 6973–2005 “test methods for single grain (precision) planter” [66]. The wide seedling strip maize no-till pneumatic seeder was assessed using a complete, randomized plot. It was 13 m wide and 100 m long (i.e., 20 rows of 100 m) with an access pathway and guard strip, and the working performances of the seeder were recorded.



**Figure 11.** Experiment field of the WNPM seeder.

##### 4.2.1. Passing Performance and Soil Disturbance

The maximum width of the seeding slot was measured using a ruler after sowing across 20 rows, taking 3 replicate sets of measurements per plot. Soil disturbance caused by the WNPM seeder was taken as the proportion of surface disturbed (GB/T 20865–2017):

$$\eta = d/D \quad (15)$$

where  $\eta$  is soil disturbance,  $d$  is width of the furrow groove, and  $D$  is row space. Furthermore, the times of blockage of machines were recorded during the replicated measurements.

##### 4.2.2. Straw Cleaning Rate on the Seedbeds’ Belt and the Residue Cover Index

Three locations (0.65 m wide and 4 m long for each) were randomly selected in the experiment plot. At each location, the straw residues on the belt of the seedbeds (0.27 m

wide and 4 m long for each seed belt) were collected and weighted before and after seeding to evaluate the quality of straw cleaning and quantity of buried straw. Meanwhile, a 100 m long and 0.65 m wide net with knots at 0.2 m intervals was used to estimate residue cover index before and after seeding. The cord was randomly placed on the surface (not parallel to the seed row), then the knots in contact with residue were counted. This procedure was carried out at 5 random locations per plot. The cover index was counted using the following equation (GB/T 20865–2017):

$$f = \frac{\sum N_2 / N_1}{5} \times 100 \quad (16)$$

where  $F$  is the cover index,  $N_1$  is the number of total knots in the 100 m long cord, and  $N_2$  is the number of total knots in contact with residue.

#### 4.2.3. Seed Singulation Performance

According to the National Standards of China, the seed singulation performances of the qualified seed spacing index, repeated sowing index, missed sowing index and sowing uniformity variation coefficient were all calculated by measuring the qualified seeding number, replayed seeding number, missed seeding number, and qualified seeding spacing index at 3 randomized 65 m long (i.e., length of ca. 260 seeding spacing) seeding rows:

$$\left\{ \begin{array}{l} A_{HG} = \frac{n_1}{N'} \times 100\% \\ D_{CB} = \frac{n_2}{N'} \times 100\% \\ L_{LB} = \frac{n_3}{N'} \times 100\% \\ CV_X = \frac{\sqrt{\frac{1}{n-1} \sum_{i=1}^n (X_i - \bar{X})^2}}{\bar{X}} \times 100\% \end{array} \right. \quad (17)$$

where  $A_{HG}$  is the qualified index of seed singulation (%),  $D_{CB}$  is the repeated index (%),  $L_{LB}$  is the missed sowing index,  $CV_X$  is the sowing uniformity coefficient of variation (%),  $n_1$  is the qualified seeding number,  $n_2$  is the repeated seeding number,  $n_3$  is the missed seeding number,  $X_i$  is the measured value of sowing spacing (mm),  $\bar{X}$  is the average value of the actual sowing spacing (mm), and  $N'$  is the theoretical total sowing number of the maize seeds.

#### 4.2.4. Seeding Depth and Plant Population

Sowing depth was also measured beside the seed singulation performance in the randomly selected three seeding rows. The qualified index and the coefficient of variation of the seeding depth can be calculated as follows (GB/T 20865–2017):

$$\left\{ \begin{array}{l} D_s = \frac{n_4}{N'} \times 100\% \\ C_V = \frac{\sqrt{\frac{1}{n-1} \sum_{i=1}^n (y_i - \bar{y})^2}}{\bar{y}} \times 100\% \end{array} \right. \quad (18)$$

where  $n_4$  is the seeding number with qualified sowing depth,  $N'$  is the theoretical total sowing number of the maize seeds,  $D_s$  is the qualified index of the sowing depth (%),  $y_i$  is the measured value of sowing depth of each sowed seed (mm),  $\bar{y}$  is the average value of the actual sowing depth (mm), and  $C_V$  is the coefficient of variation of the seeding depth. Plant population was taken as the mean of final seedling counts after seedling counts were stabilized, ~30 days after seeding.

## 5. Results and Discussion of the Field Experiment

### 5.1. Passing Performance and Soil Disturbance

As shown in Table 6, no blocking phenomenon occurs during the field experiment, and provided, on average, 265.1 mm width of seedbeds with the average soil disturbance of 38.2%. The opposite-placed anti-blocking mechanism chopped the wheat residue and the stubble on the field successfully, thus contributed to the excellent passing performance

and caused the moderate soil disturbance. The powered rake device also affected the width of seedbeds and the soil disturbance.

**Table 6.** Blocking times during the seeding, soil disturbance (%), and width of the seedbeds (mm) after the seeding.

No.	Blocking Times	Soil Disturbance	Seedbeds' Width
1	0	35.1	264.2
2	0	38.5	265.8
3	0	41.2	265.4

### 5.2. Straw Cleaning Rate

Since most of the wheat stubbles and straw in the seedling belt were effectively chopped and then buried into the soil or scattered to both sides of the seedbeds' belt by the opposite-placed anti-blocking mechanism, the straw cleaning rate achieved 94.4% in the seeding belt (as shown in Table 7). Furthermore, the powered rake device returned part of the wheat straw and residue into the soil, which also contributed to effective straw cleaning rate. However, the residue cover index of the seed plot was still over 58%, therefore, provided excellent protection from water and wind erosion in double-cropping planting system of Huang-Huai-Hai region of China [67].

**Table 7.** Wheat residue changes before and after seeding.

No.	Residue Weight before Seeding (kg/m <sup>2</sup> )	Residue Weight after Seeding (kg/m <sup>2</sup> )	Straw Cleaning Rate (%)	Residue Cover Index (%)
1	1.26	0.06	95.2	59.9%
2	1.19	0.04	96.6	58.6%
3	1.05	0.09	91.4	62.8%

### 5.3. Seed Singulation Performance

Data in Table 8 indicated that, the qualified seed spacing index of the WNPM seeder was higher than 95% at the speed of 8km/h, which is better than the maize no-till precision planter [68] with just the row cleaner and depth control unit improved, whose qualified seed spacing index was ~92% at the speed of  $\leq 6$ km/h. Generally, the design and optimization of the air suction seeder are of great significance for improving the performances of the no-till maize seeders. Meanwhile, the repeated index and missed sowing index had absolute superiors with the mean value of 0.8% and 2.6% compared with the vast variety of no-till planters [8] existing in the Huang-Huai-Hai Plain. Furthermore, the mean uniformity coefficient of variation of the seed spacing reached 19.1%, which was much superior to the requirements of  $\leq 45\%$  as stipulated in the national standards of China GB/T 20865–2017 [65]. Moreover, the missed sowing index was higher than the repeated index, which was consistent with other researches of the no till seeders [62–69], due to the fact that seed missing was more likely to occur during the seed feeding in the air suction seed meter [66].

**Table 8.** Seed singulation performance of the field experiment.

No.	Qualified Seed Spacing Index (%)	Repeated Index (%)	Missed Sowing Index (%)	Uniformity Variation Coefficient (%)
1	97.4	1.1	1.5	18.6%
2	96.7	0.5	2.8	16.9%
3	95.9	0.8	3.6	21.7%

### 5.4. Seeding Depth and Plant Population

The mean depth and its standard deviation of seed placement were 45.6 mm and 1.2 mm, respectively, while the qualified index and coefficient of variation of sowing

depth were 95.1% and 3.2%, respectively (Table 9). The results indicated that the multiple profiling devices before and after seeding of this seeder was particularly effective to maintain seeding depth. The mean depths of the seeder were closer to nominal seeding depth of 40~50 mm, and the coefficient of variation of depth was significantly smaller. The above results supported the reports from Yang et al. [68], who found that the double suppression devices improved the uniformity of sowing depth by flattening the soil before sowing and suppressing the seedling belt after sowing.

**Table 9.** Result of seeding depth.

Mean Depth (mm)	Qualified Index of Sowing Depth (%)	Standard Deviation (mm)	Coefficient of Variation (%)	Plant Population (Plant/m <sup>2</sup> )
45.6	95.1	1.2	3.2%	6.4

After the field experiment, the mean plant population was counted as 6.4 plants/m<sup>2</sup>. As shown in Figure 12, the WNPM Seeder, which equipped with opposite-placed anti-blocking mechanism, subsoiling device, powered rake device and multiple profiling devices, provided greater soil shatter around the seed belts promoted the root growth, and seedling development, which proved the results provided by Swan et al. [69] and Zhang et al. [70].



**Figure 12.** Maize emergence after the sowing in wheat straw covering filed. (a) Maize emergency, ~7 days after seeding; (b) Maize growth, ~30 days after seeding.

## 6. Conclusions

The WNPM seeder, equipped with opposite-placed anti-blocking mechanism, subsoiling device, powered rake device and multiple profiling devices, was developed to improve the operation performances at higher speed and create suitable seedbeds after wheat straw returned to the field in the double-cropping Huang-Huai-Hai Plain of China. Since the abilities of residue handling and quality of maize sowing for no-till seeders are the most significant factors for the creation of suitable seedbeds, the stubble cutting principle of opposite-placed anti-blocking mechanism and the seed filling method of pneumatic maize seed meter were theoretically analyzed, respectively. Furthermore, the structure and key parameters of the above devices were optimized through Discrete Element simulation by EDEM software.

Analyzing the capacity of the residue dealing effects through the optimization, it was determined that the shaft rotating speed of the opposite-placed anti-blocking mechanism was 500 r/min, and the spacing between each anti-blocking mechanism group was 260 mm, when the forward speed was  $\geq 8$  km/h. Meanwhile, the radius of the curve base circle of seed disc  $R_1$ , the number of shaped holes, the curvature coefficient  $\gamma$ , depth  $h_1$ , and inclined angle  $\sigma$  of the seed guide groove were determined to be 160 mm, 0.35, 34, 2.6 mm

and 20.5°, respectively, by analyzing the seed sucking ability of the seed metering with different parameters.

Finally, the working performances of the designed seeder were verified through the field experiment. Under the operating speed of 8 km/h, the seeder had excellent passing performance (no blocking) and caused the moderate soil disturbance (38.2%). Moreover, the straw cleaning rate achieved 94.4% in the seeding belt. The residue cover index of the seed plot was still over 58%. The qualified seed spacing index was higher than 95%. The qualified index of sowing depth was 95.1%, and the coefficient of variation of sowing depth was 3.2%. Compared with the existing no-till maize planter in Huang-Huai-Hai Plain, the WNPM seeder improved the working efficiency of maize sowing. Specifically, the reliable working speed increased from 5–6 km/h to more than 8 km/h, and the qualified seed spacing index went up from lower than 92% to more than 95%. In general, all the above-mentioned indexes of the WNPM seeder were much more superior to the relevant requirements as stipulated in the National Standards of China.

The designed WNPM seeder has the potential to make an important contribution to improve seed sowing quality at a high speed in Huang-Huai-Hai Plain of China. The results reported here are encouraging, and further research is needed on several aspects, including the long-term experiments, suitability of vast maize varieties, the possibility of working at the speed of  $\geq 10$  km/h, and the working performance on different cropping systems as well as in other areas.

**Author Contributions:** Conceptualization, H.L. (Hui Li) and S.S.; methodology, H.L. (Hu Liu); machine design, J.Z. and H.L. (Hui Li); EDEM software, X.Z. and R.Z.; validation, T.H. and G.W.; writing—original draft preparation, H.L. (Hui Li); writing—review and editing, H.L. (Hu Liu) and S.S.; supervision, H.Z.; funding acquisition, S.S. and H.L. (Hui Li). All authors have read and agreed to the published version of the manuscript.

**Funding:** This research was funded by Key R&D Program of Shandong Province (Major scientific and technological innovation projects), China (grant number 2019JZZY020622) and Agricultural science and technology innovation project of Shandong Academy of Agricultural Sciences (grant number CXGC2021A04).

**Institutional Review Board Statement:** Not applicable.

**Informed Consent Statement:** Not applicable.

**Data Availability Statement:** Not applicable.

**Conflicts of Interest:** The authors declare no conflict of interest.

## References

- Xu, F.L.; Guo, B.; Ye, B.; Ye, Q.; Chen, H.; Ju, X.; Guo, J.; Wang, Z. Systematical evaluation of GPMIMERG and TRMM3B42V7 precipitation products in the Huang-Huai-Hai Plain, China. *Remote Sens.* **2019**, *11*, 697. [[CrossRef](#)]
- Wu, D.; Fang, S.; Li, X.; He, D.; Zhu, Y.; Yang, Z.; Xu, J.; Wu, Y. Spatial temporal variation in irrigation water requirement for the winter wheat-summer maize rotation system since the 1980s on the North China Plain. *Agric Water Manag.* **2019**, *214*, 78–86. [[CrossRef](#)]
- NBSC (National Bureau of Statistics, China). *The Statistical Bulletin of National Economy and Social Development in China*; Peoples Republic of China, National Bureau of Statistics: Beijing, China, 2015.
- Zhang, D.; Yang, L.; Sun, S.; Dong, Y.; Zhang, D.; Xu, L.; Lu, J.; Cui, T.; Geng, D.; Li, S.; et al. Chapter I: General situation of maize production in China. In *Technology and Equipment of Mechanized Maize Production*, 1st ed.; Zhang, S., Ed.; China Agricultural University Press: Beijing, China, 2014.
- Qin, S.; Liang, L.; Xiang, L.; Hui, L.; Zhang, L. Dynamic analysis of drought trend in Huang-huai-hai region based on MODIS and TVDI. In *IGARSS 2016—2016 IEEE International Geoscience and Remote Sensing Symposium*; IEEE: Beijing, China, 2016.
- Li, H.W.; Gao, H.W.; Wu, H.D.; Li, W.Y.; Wang, X.Y.; He, J. Effects of 15 years of conservation tillage on soil structure and productivity of wheat cultivation in northern China. *Aust. J. Soil Res.* **2007**, *45*, 344–350. [[CrossRef](#)]
- Li, H.W.; He, J.; Gao, H.W.; Chen, Y.; Zhang, Z.Q. The effect of conservation tillage on crop yield in China. *Front. Agric. Sci. Eng.* **2015**, *2*, 179–185.
- He, J.; Li, H.; McHugh, A.D.; Wang, Q.; Lu, Z.; Li, W.; Zhang, Y. Permanent raised beds improved crop performance and water use on the North China Plain. *J. Soil Water Conserv.* **2015**, *70*, 54–62. [[CrossRef](#)]

9. He, J.; Li, H.W.; Chen, H.T.; Lu, C.Y.; Wang, Q. Research Progress of Conservation Tillage Technology and Machine. *Trans. Chin. Soc. Agric. Mach.* **2018**, *49*, 1–19.
10. Gao, W.S. Development trends and basic principles of conservation tillage. *Sci. Agric. Sin.* **2007**, *40*, 2702–2708.
11. Zhu, G.H.; Li, W.Y.; He, J. Design and experiment on 2BFML-5 no-till planter for permanent raised bed. *Trans. Chin. Soc. Agric. Mach.* **2008**, *2*, 51–54.
12. Li, H.W.; Chen, J.D.; Deng, J.; Zhao, W.D. Study on technology and machines of mechanized conservation tillage for dryland maize. *J. China Agric. Univ.* **2000**, *4*, 68–72.
13. Yao, Z.L.; Gao, H.W.; Wang, X.Y. Design and experiment on 2BMX-5 No-till Wheat-maize Seeder. *Trans. Chin. Soc. Agric. Mach.* **2008**, *39*, 64–68.
14. Chen, H.; Huang, H.; Yang, Y.L.; Li, H.W. Design of Row-followed No-till Wheat and Maize Planter under Controlled Traffic Farming System. *Trans. Chin. Soc. Agric. Mach.* **2009**, *40*, 72–76.
15. Zhang, X.R.; He, J.; Li, H.W.; Wang, Q.J.; Wu, S.S. Design and experiment on No-till Planter in Horizontal Residue-throwing Finger-wheel type for maize. *Trans. Chin. Soc. Agric. Mach.* **2010**, *41*, 39–43.
16. Zhang, J.C.; Yan, X.L.; Xue, S.P.; Zhu, R.X.; Su, G.Y. Design of No-tillage Maize Planter with Straw Smashing and Fertilizing. *Trans. Chin. Soc. Agric. Mach.* **2012**, *43*, 51–55.
17. Yang, Z.D.; Liu, N.N.; Geng, D.Y.; Chai, S.; Ma, M.J.; Du, R.C. Design and Experiment on Type 2BYM-12 Folding and Dynamic Anti-blocking No-till Planter. *Trans. Chin. Soc. Agric. Mach.* **2013**, *44*, 46–50.
18. Li, F.H.; Du, R.C.; Diao, P.S.; Zhang, Y.P.; Cui, Q.; Li, T. Design and Experiment of Helm-shaped No-tillage Precision Fertilization Planter for Corn. *Trans. Chin. Soc. Agric. Mach.* **2013**, *44*, 33–38.
19. Gao, N.N.; Zhang, D.X.; Yang, L.; Liu, J.; Cui, T. Design and experiment of drum-type anti-blocking mechanism of no-till planter for maize. *Trans. Chin. Soc. Agric. Eng.* **2012**, *28*, 31–37.
20. Cao, X.P.; Wang, Q.J.; Li, H.W.; He, J.; Lu, C.Y. Combined Row Cleaners Research with Side Cutter and Stubble Clean Disk of Corn No-till Seeder. *Trans. Chin. Soc. Agric. Mach.* **2021**, *52*, 36–44.
21. Wang, W.W.; Zhu, C.X.; Chen, L.Q.; Li, Z.D.; Huang, X.; Li, J.C. Design and experiment of active straw-removing anti-blocking device for maize no-tillage planter. *Trans. Chin. Soc. Agric. Mach.* **2017**, *33*, 10–17.
22. Yao, W.Y.; Zhao, D.B.; Xu, G.F.; Chen, M.Z.; Miao, H.Q.; Diao, P.S. Design and Experiment of Anti-blocking Device for Strip to row Active Corn No-tillage Seeding. *Trans. Chin. Soc. Agric. Mach.* **2020**, *51*, 55–62, 71.
23. Siemens, M.C.; Wilkins, D.E.; Correa, R.F. Development and evaluation of a residue management wheel for hoe-type no-till drills. *Trans. Am. Soc. Agric. Eng.* **2004**, *47*, 397–404. [[CrossRef](#)]
24. Niu, M.M.; Fang, H.M.; FA, C.; Shi, S.; Xue, Y.; Liu, H. Design and Experiment of Separating-guiding Anti-blocking Mechanism for No-tillage Maize Planter. *Trans. Chin. Soc. Agric. Mach.* **2019**, *50*, 52–58.
25. Li, Y.; Yan, B.; Yu, Y.; He, X.; Liu, Q.; Liang, Z.; Yin, X.; Cui, T.; Zhang, D. Global overview of research progress and development of precision maize planters. *Int. J. Agric. Biol. Eng.* **2016**, *9*, 9–26.
26. Hudspeth, E.B.; Wanjura, D.F. A planter for precision depth and placement of cotton seed. *Trans. ASAE* **1970**, *13*, 153–155. [[CrossRef](#)]
27. Karayel, D.; Barut, Z.B.; Özmerzi, A. Mathematical modelling of vacuum pressure on a precision seeder. *Biosyst. Eng.* **2004**, *87*, 437–444. [[CrossRef](#)]
28. Karayel, D. Performance of a modified precision vacuum seeder for no-till sowing of maize and soybean. *Soil Tillage Res.* **2009**, *104*, 121–125. [[CrossRef](#)]
29. John Deere No-Till Air Dill. Available online: <https://www.deere.com/en/seeding-equipment/> (accessed on 12 August 2021).
30. Vaderstad Tempo. Available online: <https://www.vaderstad.com/en/planting/tempo-planter/tempo-r-4-6/> (accessed on 15 August 2021).
31. Fallahi, S.; Raoufat, M.H. Row-crop planter attachments in a conservation tillage system: A comparative study. *Soil Tillage Res.* **2008**, *98*, 27–34. [[CrossRef](#)]
32. Swan, J.B.; Higgs, R.L.; Bailey, T.B.; Wollenhaupt, N.C.; Paulson, W.H.; Peterson, A.E. Surface residue an in-row treatment effects on long-term no-tillage and continuous corn. *Agron. J.* **1994**, *86*, 711–718. [[CrossRef](#)]
33. Nafziger, D.; Carter, P.R.; Graham, E.E. Response of corn to uneven emergence. *Crop Sci.* **1991**, *31*, 811–815. [[CrossRef](#)]
34. Ford, J.H.; Hicks, D.R. Corn growth and yield in uneven emerging stands. *J. Prod. Agric.* **1992**, *5*, 185–188. [[CrossRef](#)]
35. Mead, J.A.; Chan, K.Y. Effect of deep tillage and seedbed preparation on the growth and yield of wheat on a hard-setting soil. *Aust. J. Exp. Agric.* **1988**, *28*, 491–498. [[CrossRef](#)]
36. Yao, Z.; Li, H.; Gao, H.; Wang, X.; HE, J. Crop performance as affected by three opening configurations for no-till seeder in annual double cropping regions of northern China. *Soil Res.* **2010**, *47*, 839–847. [[CrossRef](#)]
37. Loon, J.V.; Krupnik, T.J.; López-Gómez, J.A.; Timsina, J.; Govaerts, B.A. Standard methodology for evaluation of mechanical maize seed meters for smallholder farmers comparing devices from latin america, sub-saharan africa, and asia. *Agronomy* **2020**, *10*, 1091. [[CrossRef](#)]
38. Timsina, J.; Jat, M.L.; Majumdar, K. Rice-maize systems of South Asia: Current status, future prospects and research priorities for nutrient management. *Plant Soil* **2010**, *335*, 65–82. [[CrossRef](#)]
39. Timsina, J.; Buresh, R.J.; Dobermann, A.; Dixon, J. *Rice-Maize Systems in Asia: Current Situation and Potential*; CIMMYT, IRRI: Los Baños, Phillipines, 2011; p. 235.

40. Jin, H.; Li, H.; Wang, Q.; Gao, H.; Li, W.; Zhang, X.; MCGiffen, M. The adoption of conservation tillage in China. *Ann. N. Y. Acad. Sci.* **2010**, *1195*, 96–106.
41. Jin, H.; Zhang, Z.; Li, H.; Wang, Q. Development of small/medium size no-till and minimum-till seeders in Asia: A review. *Int. J. Agric. Biol. Eng.* **2014**, *7*, 1–12.
42. National Standardization Administration Committee of China; General Administration of Quality Supervision, Inspection and Quarantine of the People's Republic of China. *GB/T 5669–2017 Rotary Tillage Machinery Knife and Knife Holder*; Standards Press of China: Beijing, China, 2017.
43. Chinese Academy of agricultural mechanization. *Design Manual of Agricultural Machinery*; China Agricultural Science and Technology Press: Beijing, China, 2007.
44. Matin, M.A.; Fielke, J.M.; Desbiolles, J.M.A. Furrow parameters in rotary strip-tillage: Effect of blade geometry and rotary speed. *Biosyst. Eng.* **2014**, *118*, 7–15. [[CrossRef](#)]
45. Zhang, J.G.; Gao, H.W.; Yang, G. Study on the chopping property of wheat straw. *Trans. Chin. Soc. Agric. Eng.* **2000**, *16*, 70–72.
46. Shi, S.; Zhou, J.L.; Liu, H.; Fang, H.M.; Jian, S.C.; Zhang, R.F. Design and Experiment of Pneumatic Precision Seed-metering Device with Guided Assistant Seed-filling. *Trans. Chin. Soc. Agric. Mach.* **2019**, *50*, 61–70.
47. Cundall, P.; Strack, O. A discrete numerical model for granular assemblies. *Geotechnique* **1979**, *29*, 47–65. [[CrossRef](#)]
48. Coetzee, C.J.; Lombard, S.G. The destemming of grapes: Experiments and discrete element modelling. *Biosyst. Eng.* **2013**, *114*, 232–248. [[CrossRef](#)]
49. González-Montellano, C.; Ayuga, F.; Ooi, J. Discrete element modelling of grain flow in a planar silo: Influence of simulation parameters. *Granul. Matter.* **2011**, *13*, 149–158.
50. Lenaerts, B.; Aertsen, T.; Tijskens, E.; Ketelaere, B.D.; Ramon, H.; Baerdemaeker, J.D.; Saeys, W. Simulation of grain–straw separation by Discrete Element Modeling with bendable straw particles. *Comput. Electron. Agric.* **2014**, *101*, 24–33. [[CrossRef](#)]
51. Van Liedekerke, P.; Tijskens, E.; Dintwa, E.; Rioual, F.; Vangeyte, J.; Ramon, H. DEM simulations of the particle flow on a centrifugal fertilizer spreader. *Powder Technol.* **2009**, *190*, 348–360. [[CrossRef](#)]
52. Mak, J.; Chen, Y.; Sadek, M.A. Determining parameters of a discrete element model for soil-tool interaction. *Soil Tillage Res.* **2012**, *118*, 117–122. [[CrossRef](#)]
53. Han, D.; Zhang, D.; Jing, H.; Li, Y.; Tao, C.; Ding, Y.; Wang, Z.; Wang, Y.; Zhang, T. Dem-CFD coupling simulation and optimization of an inside-filling air-blowing maize precision seed-metering device. *Comput. Electron. Agric.* **2018**, *150*, 426–438. [[CrossRef](#)]
54. Lei, X.; Liao, Y.; Liao, Q. Simulation of seed motion in seed feeding device with DEM-CFD coupling approach for rapeseed and wheat. *Comput. Electron. Agric.* **2016**, *131*, 29–39. [[CrossRef](#)]
55. Bravo, E.L.; Tijskens, E.; Suárez, M.H.; Cueto, O.G.; Ramon, H. Prediction model for non-inversion soil tillage implemented on discrete element method. *Comput. Electron. Agric.* **2014**, *106*, 120–127. [[CrossRef](#)]
56. Chen, Y.; Munkholm, L.J.; Nyord, T. A discrete element model for soil–sweep interaction in three different soils. *Soil Tillage Res.* **2013**, *126*, 34–41. [[CrossRef](#)]
57. Asaf, Z.; Rubinstein, D.; Shmulevich, I. Determination of discrete element model parameters required for soil tillage. *Soil Tillage Res.* **2007**, *92*, 227–242. [[CrossRef](#)]
58. Jiang, M.; Liu, C.; Wei, D.; Du, X.; Cai, P.; Song, J. Design and Test of Wide Seedling Strip Wheat Precision Planter. *Trans. Chin. Soc. Agric. Mach.* **2019**, *50*, 53–61.
59. Wang, X.L.; Hu, H.; Wang, Q.J.; Li, H.; Chen, W. Calibration Method of Soil Contact Characteristic Parameters Based on DEM Theory. *Trans. Chin. Soc. Agric. Mach.* **2017**, *48*, 78–85.
60. Fang, H.M. *Research on the Straw-Soil-Rotary Blade Interaction Using Discrete Element Method*; Nanjing Agricultural University: Nanjing, China, 2016; pp. 33–97.
61. Fang, H.; Shi, S.; Qiao, L.; Niu, M.; Xu, G.; Jian, S. Numerical and experimental study of working performance of round roller-claw type anti-blocking mechanism. *J. Chin. Agric. Mech.* **2018**, *39*, 01–09.
62. Yang, Q.L.; Li, Z.H.; Li, H.W.; Jin, H.E.; Wang, Q.; Lu, C.Y.; China Agricultural University. Numerical analysis of particle motion in pneumatic centralized fertilizer distribution device based on CFD DEM. *Trans. Chin. Soc. Agric. Mach.* **2019**, *50*, 81–89.
63. Shi, S.; Liu, H.; Wei, G.; Zhou, J.; Jian, S. Optimization and Experiment of Pneumatic Seed Metering Device with Guided Assistant Filling Based on EDEM CFD. *Trans. Chin. Soc. Agric. Mach.* **2020**, *51*, 54–66.
64. Zhang, J.; Li, X.M.; Mou, H.Q. The application of response model methodology in product design improvement. *Appl. Stat. Manag.* **2004**, *23*, 43–48.
65. National Standardization Administration Committee of China; General Administration of Quality Supervision, Inspection and Quarantine of the People's Republic of China. *GB/T 20865–2017 No/Less Tillage and Fertilization Seeding*; China Standard Press: Beijing, China, 2017.
66. Ministry of Industry and Information Technology of the People's Republic of China. *GB/T 6973–2005 Test Method for Single Grain (Precision) Planter*; China Standards Press: Beijing, China, 2006.
67. Liu, L.J. *Systematic Experiments and Effect Analysis of All Year Conservation Tillage in Two Crops a Year Region*; China Agricultural University: Beijing, China, 2004.
68. Yang, L.; Zhang, R.; Liu, Q.W.; Yin, X.W.; He, X.T.; Cui, T.; Zhang, D.X. Row cleaner and depth control unit improving sowing performance of maize no-till precision planter. *Trans. Chin. Soc. Agric. Eng.* **2016**, *32*, 18–23.

- 
69. Swan, J.B.; Kaspar, T.C.; Erbach, D.C. Seed-row residue management for corn establishment in the northern US Corn Belt. *Soil Tillage Res.* **1996**, *40*, 55–72. [[CrossRef](#)]
  70. Zhang, J.X.; Liu, C.Y.; Shi, J.L.; Jing, M.; Wang, F. Effects of no tillage with stubble mulch on sowing and seedling of spring wheat in the Hexi Irrigation Area. *J. Gansu Agric. Univ.* **2006**, *4*, 31–34.